

SWIR/MWIR InP-Based p-i-n Photodiodes with InGaAs/GaAsSb Type-II Quantum Wells

Baile Chen, Weiyang Jiang, Jinrong Yuan, Archie L. Holmes, Jr., and Bora. M. Onat

Abstract—This paper presents the performance characteristics of InP-based p-i-n photodiodes with strain-compensated and lattice-matched InGaAs/GaAsSb type-II multiple quantum well (MQW) absorption regions. The results show that photodiodes with strain-compensated and lattice-matched absorption regions have optical response out to 3.4 and 2.8 μm with dark current densities of 9.7 and 1.66 mA cm^{-2} , respectively, at 290 K under -0.5 V reverse bias. The carrier transport mechanism responsible for the difference in responsivity and detectivity between strain-compensated and lattice-matched InGaAs/GaAsSb MQWs is discussed.

Index Terms—Detectivity, GaAsSb, InGaAs, mid-wavelength infrared, p-i-n photodiode, short-wavelength infrared, type-II multiple quantum wells.

I. INTRODUCTION

SHORT-WAVE infrared (SWIR) and Mid-wave infrared (MWIR) photodetectors have applications in areas such as chemical sensing, gas monitoring, medical diagnostics, infrared imaging and free-space communications. Mercury Cadmium Telluride (HgCdTe) is the predominant material system used in MWIR and long-wave infrared (LWIR) applications [1]. However, HgCdTe often suffers from poor material uniformity and low yield [2]. Comparable performance can be achieved on GaSb substrate with high quality InAs/GaSb strained-layer superlattices, but significant cooling is required for high detectivity [3]–[5]. Bulk InAs based devices with a cut-off wavelength of 3.6 μm , is another option for MWIR detection, but the dark current performance degrades significantly at room temperature [6], [7]. Also, for imaging applications InAs based photodiodes require the substrate to be thinned for post hybridization to a readout integrated circuit, which is a low yield, and cumbersome process.

InP-based materials have been used to make high performance photonics devices in the 1.1 μm –1.6 μm wavelength range. Longer detection wavelengths can be achieved using mismatched InGaAs [8], [9]. For example, Hamumatsu sells

Manuscript received February 25, 2011; revised May 27, 2011; accepted June 11, 2011. Date of current version August 16, 2011. This work was supported in part by the Army Research Office and the National Science Foundation under Grant 0912672 and Grant 0907236 monitored by Dr. W. Clark.

B. Chen, W. Y. Jiang, J. Yuan, and A. L. Holmes are with the Department of Electrical and Computer Engineering, University of Virginia, Charlottesville, VA 22904-4743 USA (e-mail: bc4fm@virginia.edu; weiyang99@yahoo.com; jy8q@virginia.edu; ah7sj@virginia.edu).

B. M. Onat is with the Princeton Lightwave Inc., Cranbury, NJ 08512 USA (e-mail: bmonat@princetonlightwave.com).

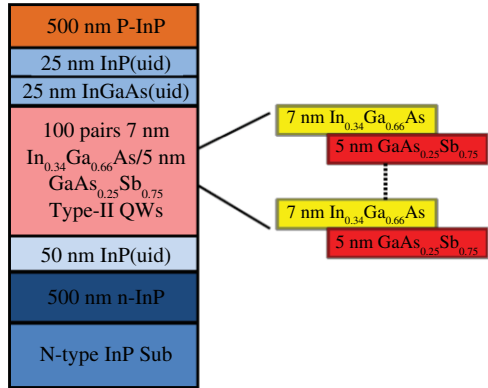
Color versions of one or more of the figures in this paper are available online at <http://ieeexplore.ieee.org>.

Digital Object Identifier 10.1109/JQE.2011.2160450

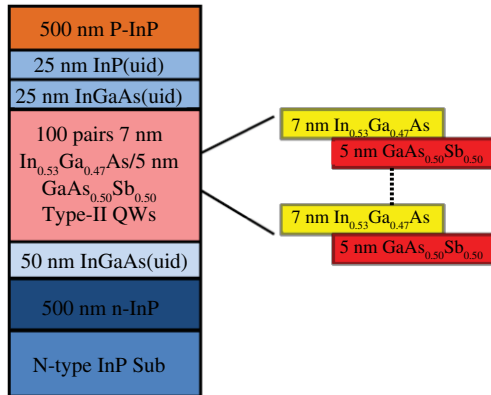
a uncooled device with a maximum detection wavelength of 2.6 μm , dark current densities between 0.6 and 5 mA/cm^2 depending on device area, responsivities around 1.3 A/W, and a specific detectivity of $5 \times 10^{10} \text{ cm}\cdot\text{Hz}^{1/2}\cdot\text{W}^{-1}$ [9]. Our approach to achieving longer wavelength detection is to use InGaAs/GaAsSb type-II multiple quantum wells (MQWs) as the absorption region. In the InGaAs-GaAsSb type-II quantum well structure, electrons are confined in the conduction band of the InGaAs layer, while holes are confined in the valence band of GaAsSb layer. This type-II band line-up has a narrower effective bandgap than type-I transitions and can enable longer wavelength detection. Sidhu et. al. [10] initially demonstrated an InP-based p-i-n photodiode using 150 pairs of lattice matched InGaAs/GaAsSb MQWs with a peak detectivity of $3.8 \times 10^9 \text{ cm}\cdot\text{Hz}^{0.5}\cdot\text{W}^{-1}$ at room temperature at 2.26 μm . Inada et. al. [11] used 250 pairs of those quantum wells as the absorption region to achieve the responsivity 0.6 A/W at 2.2 μm with dark current density of 0.92 mA/cm^2 . The InP-based separate-absorption-multiplication (SAM) APD using lattice matched InGaAs/GaAsSb type-II quantum wells as the absorption region were also reported [12], [13]. In all of the cases listed above, lattice matched quantum wells were used as the absorption region. To extend the wavelength, strain or strain compensation needs to be added [14]–[16]. In this work, we compare two photodiodes: one using lattice-matched materials and the other using strain compensation to move the detection wavelength into the MWIR. Our results show that the longer wavelength detection can be achieved with the strain compensated structures at the expense of a modest increase in dark current.

II. PHOTODIODE DESIGN AND FABRICATION

Two different p-i-n photodiodes were designed, epitaxially grown in an MBE reactor, fabricated, and characterized. The strain compensated design (Sample A) has one hundred pairs of 7 nm $\text{In}_{0.34}\text{Ga}_{0.66}\text{As}/5$ nm $\text{GaAs}_{0.25}\text{Sb}_{0.75}$ as shown below in Figure 1(a). This structure was designed for MWIR detection (3.4 μm). In our previous work, we determined that the optimal strain compensated design should use compressively strained GaAsSb and tensile strained InGaAs with the thickness of the GaAsSb layers being thinner than the InGaAs layers [15], [16]. As a direct comparison, a lattice-matched structure with one hundred pairs of 7 nm $\text{In}_{0.53}\text{Ga}_{0.47}\text{As}/5$ nm $\text{GaAs}_{0.5}\text{Sb}_{0.5}$ (Sample B) was designed as shown in Figure 1(b), which has optical response up to 2.8 μm . Based on these designs, transitions between the lowest energy states



(a)



(b)

Fig. 1. (a) Schematic of the p-i-n device structure with type-II 7-nm $\text{In}_{0.34}\text{Ga}_{0.66}\text{As}/5\text{-nm GaAs}_{0.25}\text{Sb}_{0.75}$ MQWs as absorption layer (Sample A). (b) Schematic of the p-i-n device structure with type-II 7-nm $\text{In}_{0.53}\text{Ga}_{0.47}\text{As}/5\text{-nm GaAs}_{0.5}\text{Sb}_{0.5}$ MQWs as absorption layer (Sample B).

in the InGaAs and GaAsSb for both devices are expected to occur around 0.38 eV and 0.47 eV respectively.

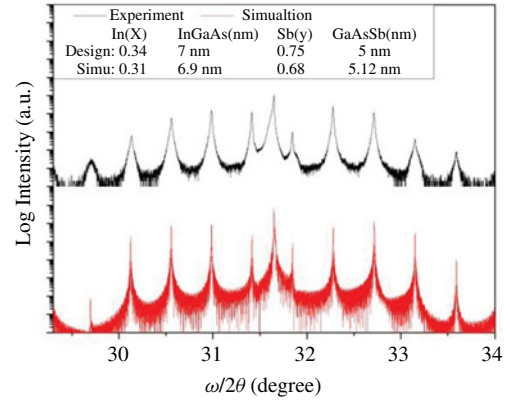
Material composition and thickness of layers were verified using high resolution X-ray diffraction (HRXRD) as shown in Figure 2. The appearances of a large number of satellite peaks suggest that both structures are of high quality and have abrupt interfaces in the absorption region. The full-width at half-maximum (FWHM) of the satellite peak of Sample A are larger than the simulation suggesting that some strain relaxation may be occurring.

Devices with top-illuminated mesas were fabricated from both structures using conventional photolithography and lift-off techniques. The circular device mesa was etched with 3% Br: CH_3OH and H_3PO_4 : H_2O_2 : H_2O (1 : 1 : 10). A 200 nm of plasma-enhanced chemical vapor deposition (PECVD) SiO_2 was used as a passivation layer and Cr (40 nm)-Au (100 nm) were deposited by e-beam evaporator to form the n- and p-contacts.

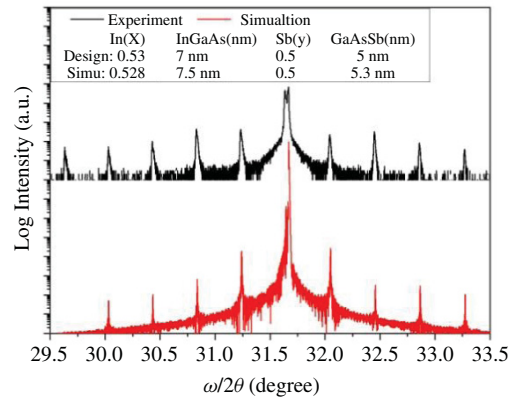
III. EXPERIMENTAL RESULTS

A. DC Characteristics

The dark current-voltage (I-V) characteristics of thirty (30) devices of both samples were measured at 200 K. Twenty-



(a)



(b)

Fig. 2. (a) HRXRD $\omega/2\theta$ of sample A with 100 pairs of 7-nm $\text{In}_{0.34}\text{Ga}_{0.66}\text{As}/5\text{-nm GaAs}_{0.25}\text{Sb}_{0.75}$. (b) HRXRD $\omega/2\theta$ of sample B with 100 pairs of 7-nm $\text{In}_{0.53}\text{Ga}_{0.47}\text{As}/5\text{-nm GaAs}_{0.5}\text{Sb}_{0.5}$.

one (21) of the devices from Sample A and twenty-nine (29) of the devices from Sample B show the similar dark current characteristics with very low variation. We believe that the variations in performance are due to wafer non-uniformity.

Devices with 180 μm diameters from both samples were selected and wire bonded for the characterization at different temperatures as shown in Figure 3(a) and Figure 3(b). Device A and Device B have dark current densities of 9.7 mA/cm^2 and 1.66 mA/cm^2 at 290 K at -0.5 V, and decrease to 58.6 $\mu\text{A}/\text{cm}^2$ and 4.89 $\mu\text{A}/\text{cm}^2$ at 200 K, respectively.

The higher dark current may be due to the fact that there is a higher thermal generation-recombination rate in the absorption region due to the smaller effective bandgap in Sample A. In addition, Figure 3 demonstrates that the dark current drops rapidly with temperature for both devices. This suggests that the dominant mechanism for dark current in this regime is the thermal generation of carriers. This was confirmed by observing that the change in dark current scales close to device area as opposed to perimeter. An Arrhenius plot of the dark current for both devices is shown in Figure 4. A good exponential fit to the data suggests that a single activation energy dominates the dark current. For the fit, the activation energy is 0.282 eV and 0.319 eV for Device A and B respectively.

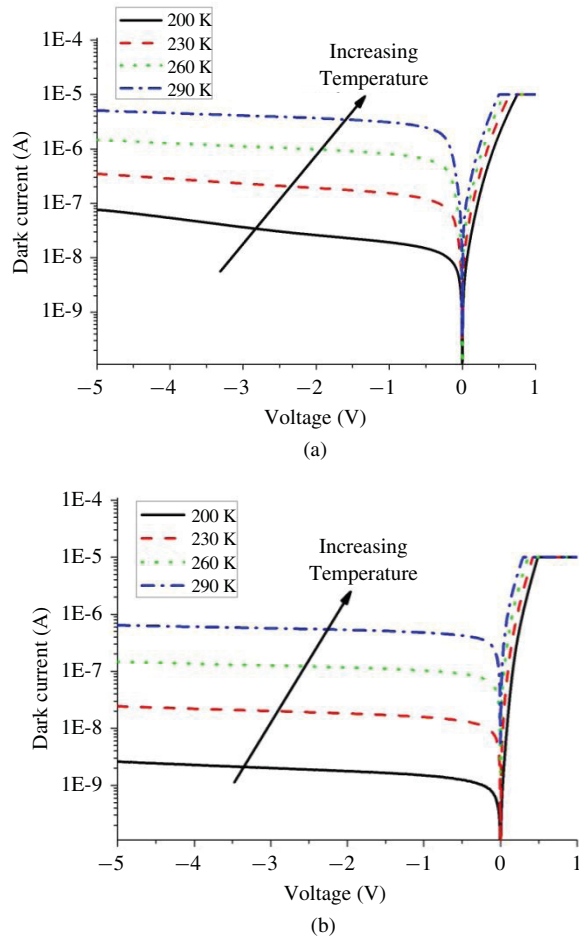


Fig. 3. (a) Dark current versus voltage for a 180- μm diameter Device A measured at different temperatures. (b) Dark current versus voltage for a 180- μm diameter Device B measured at different temperatures.

B. Optical Characteristics

A Nichlet Magna-II Fourier transform infrared (FTIR) spectrometer with a low-noise current preamplifier was used to measure the relative spectral response. Since the radiation from blackbody at certain temperature is given by Planck's radiation law, the absolute responsivity of this device was calibrated using a blackbody source maintained at 700 °C (in order to have radiation power peak at around 3 μm) with a chopper at a modulation frequency of 150 Hz, a current preamplifier, and a Fast Fourier Transform (FFT) spectrum analyzer. An 1800-nm long pass filter was placed between the blackbody source and the device to eliminate the contribution to the responsivity from spatially direct absorption in the InGaAs and GaAsSb layers.

The normal incident photo response was measured at temperatures between 200 K and 290 K. The results are shown in Figure 5. As expected, Device A has an optical response out to a longer wavelength than Device B (3.4 μm versus 2.8 μm) and the response increases with temperature because the photo generated carries will have more thermal energy to transport over the hetero-barriers and transit to the electrodes. There is a significant dip around 2.0 μm for Device B, the cause of this dip is not clear yet and needs further investigations.

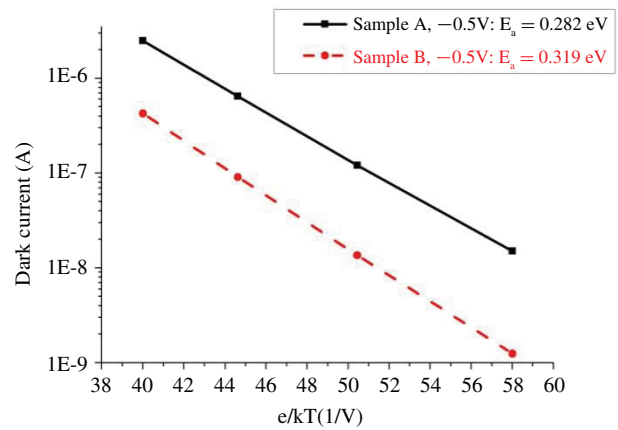


Fig. 4. Arrhenius plot of the dark current for 180- μm diameter Devices A and B at reverse bias -0.5 V.

To optimize the performance of these devices, the blackbody responsivity (BR) under different reverse biases and temperatures was measured and plotted in Figure 6. Here the blackbody responsivity is defined as the output photo current of device produced in response to a watt of input optical radiation from a blackbody source at 700 °C. This blackbody response can be used to determine the absolute value of responsivity and it is proportional to the absolute value of responsivity, when the relative responsivity of device is known by the measurement of FTIR spectrometer.

As shown in Figure 6, the blackbody responsivity of Device A is larger than that of Device B which is due to the fact that Device A has wider absorption window and higher response in the blackbody spectrum. For reverse biases above 0.5 V, the blackbody responsivity for both devices increases with temperature. However, the blackbody responsivity at small reverse biases initially increases with temperature and then decreases after some critical temperature. This critical temperature for Device A is 140 K and 230 K for reverse biases of 0 V and -0.2 V respectively. While this effect is not completely understood at this time, we believe that temperature and bias dependence of the thickness of depletion region in the absorption region may be the main cause of this effect. At high temperature and under zero bias or small bias, the absorption region may be not fully depleted due to the unintentional doping concentration, and the carriers generated outside the depletion region will recombine before they are collected. As the temperature decrease, the overall background doping concentration in absorption region drops due to incomplete dopant ionization, thus, the absorption region would be more depleted at small bias, which helps collect the photo generated carriers. Moreover, the fact that the carrier lifetime also increase as temperature decreases also benefits the carrier collection.

The blackbody responsivity of Device B shows similar behavior with higher critical temperatures. At zero bias, the critical temperature of Device B is around 260 K. That is due to the fact that at the same temperature, the background

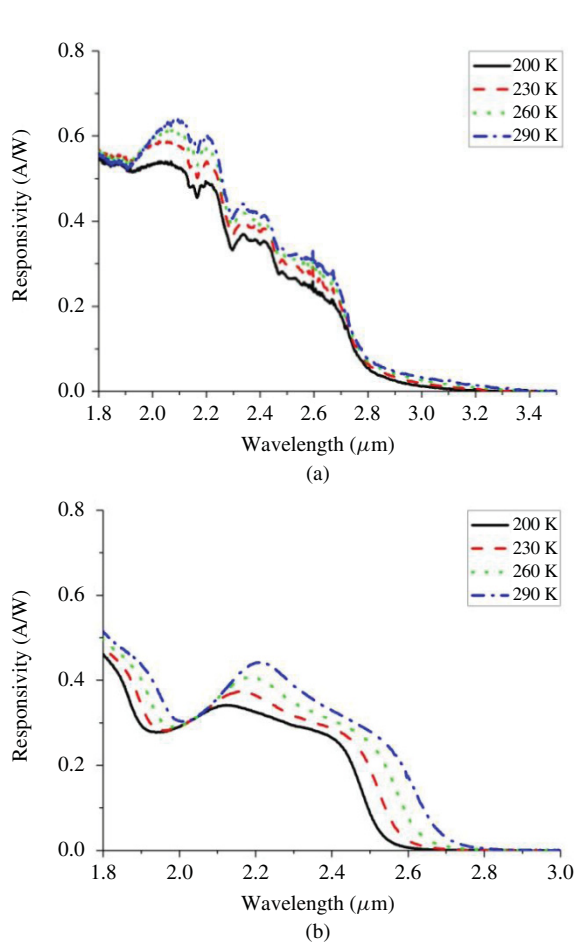


Fig. 5. (a) Normal-incidence photoresponse of the device under different temperatures at a reverse bias of -0.5 V for Device A. (b) Normal-incidence photoresponse of the device under different temperatures at a reverse bias of -0.5 V for Device B.

doping density in the absorption region of Device B is lower, and the carrier life time in Device B is longer, compared with Device A. We believe that the slight strain relaxation observed in Device A is the cause of a reduction in carrier lifetime.

Furthermore, the blackbody responsivity of both devices is almost independent of the reverse bias at temperatures below 140 K and 230 K respectively. That is because at low temperature, the absorption region are fully depleted even at small bias, and the photo generated carriers also have long enough lifetime to be swept out of the depletion region even by the small electrical field.

To measure the detectivity of these devices, the dark current noise of the device was characterized using the similar procedure as the responsivity. To obtain this data, the device was mounted on a cold finger inside a cryostat and the cryostat chamber was covered to eliminate stray light from shining on the device. The noise current from the device was amplified using a pre-amplifier. An FFT spectrum analyzer was used to view the noise spectrum. This measurement system has a noise floor around $1 \times 10^{-14} \text{ A}/\text{Hz}^{1/2}$. The noise spectrum densities versus the temperature for both devices under -0.5 V are shown in Figure 7. As shown the noise of Device A is

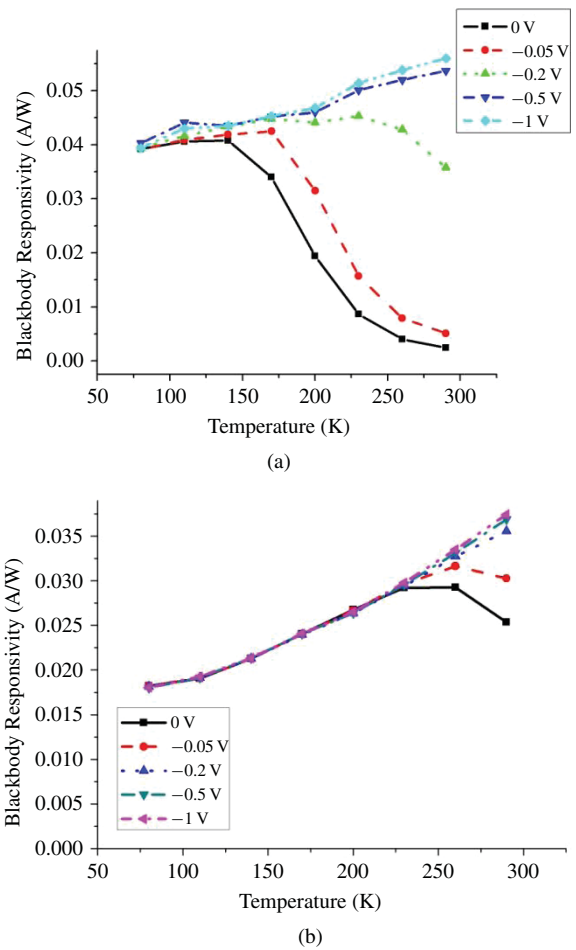


Fig. 6. (a) Blackbody responsivity versus temperature under different reverse bias for Device A. (b) Blackbody responsivity versus temperature under different reverse bias for Device B. These responses have been filtered by a long-pass filter of 1800 nm.

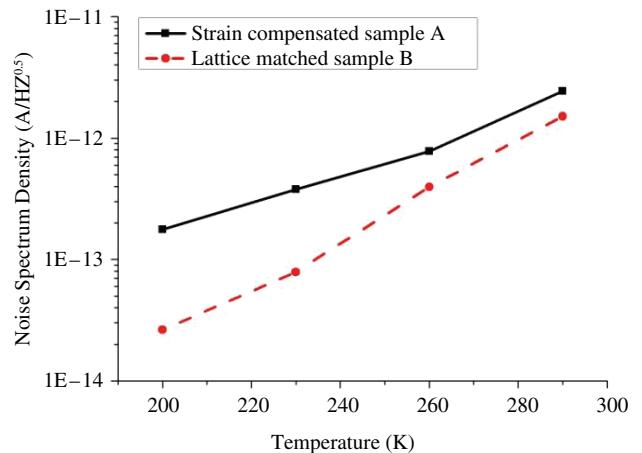


Fig. 7. Dark noise spectrum densities versus temperature under reverse bias of -0.5 V for Devices A and B.

higher than that of Device B, and the difference between each other increases as the temperature decreases.

The device's specific detectivity (D^*) as a function of wavelength is calculated from the responsivity and noise with

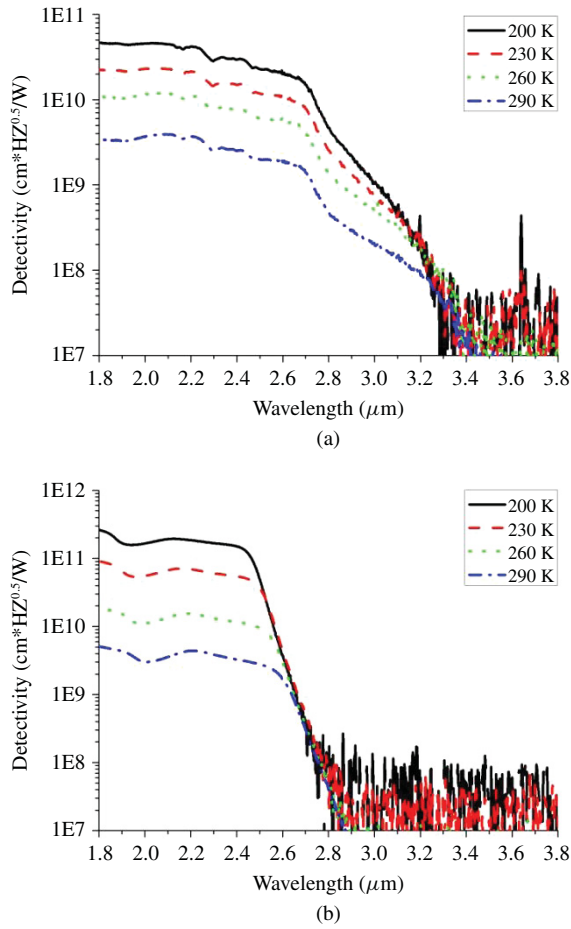


Fig. 8. (a) Detectivity of Device A at different temperatures under a reverse bias of -0.5 V. (b) Detectivity of Device B at different temperatures under a reverse bias of -0.5 V.

the following formula [17]:

$$D^* = \frac{R \cdot \sqrt{A_d}}{S_n} \quad (1)$$

where R is the responsivity, A_d is the diode area and S_n is the noise spectrum density. The D^* versus wavelength for both devices at different temperature is shown in Figure 8(a) and 8(b). D^* for Device A is $2.0 \times 10^8 \text{ cm} \cdot \text{Hz}^{1/2} \cdot \text{W}^{-1}$ at $\lambda = 3.0 \mu\text{m}$ at 290 K and increases to $1.0 \times 10^9 \text{ cm} \cdot \text{Hz}^{1/2} \cdot \text{W}^{-1}$ at 200 K. Moreover, D^* for Device B is $2.79 \times 10^9 \text{ cm} \cdot \text{Hz}^{1/2} \cdot \text{W}^{-1}$ at $\lambda = 2.5 \mu\text{m}$ at 290K and increases to $4.96 \times 10^{10} \text{ cm} \cdot \text{Hz}^{1/2} \cdot \text{W}^{-1}$ at 200 K. The room temperature D^* of Device B is smaller than the relaxed InGaAs photodiodes with cut-off wavelength at $2.6 \mu\text{m}$ shown in [18]. We believe higher detectivities are possible to be achieved with a thicker absorption region and lower operation bias.

To further investigate the optimum performance of the Device A under different reverse biases, the noise current spectrum densities at room temperature were measured as a function of reverse bias as shown in Figure 9. The blackbody responsivity (BR) and blackbody detectivity (BD^*) versus the reverse bias are shown in Figure 10, in which the blackbody

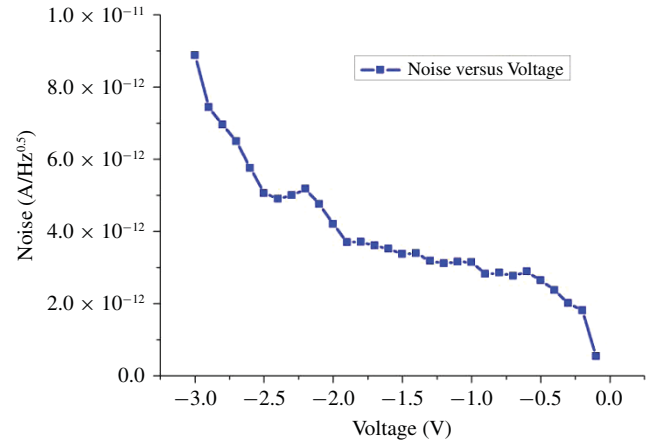


Fig. 9. Noise versus reverse bias for a $180\text{-}\mu\text{m}$ diameter Device A measured at room temperature.

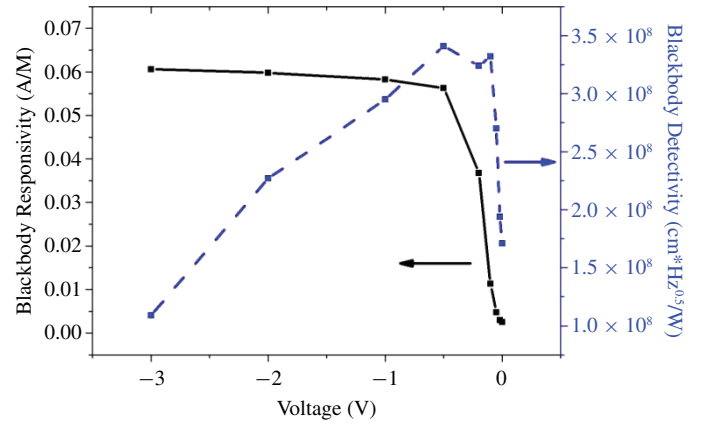


Fig. 10. Blackbody responsivity and blackbody detectivity of Device A versus reverse bias for a $180\text{-}\mu\text{m}$ diameter device measured at room temperature.

detectivity is defined as:

$$BD^* = \frac{BR \cdot \sqrt{A_d}}{S_n} \quad (2)$$

In Figure 10, blackbody responsivity increases positively with reverse bias. However, responsivity will saturate when the reverse bias is higher than -0.5 V, since the total number of e-h pair generated is roughly constant regardless of increase in the reverse bias. Furthermore, Figure 10 demonstrates that the device achieves optimum performance with a reverse bias around -0.5 V. If the voltage is increased, the noise of the device increases more rapidly than responsivity increases for the device. For lower biases, the optical response drops faster than the reduction in the device noise.

If the operation temperature of the Device A is reduced to 200 K, the optimized reverse bias decreases to 0.2 V because of the smaller bias required to depleted the absorption region and the increased life time of photo generated carriers in the absorption region at 200 K. Similar phenomena happened to Device B. But the optimized operation reverse bias of Device B at room temperature is around -0.05 V (not -0.5 V), since Device B have lower back ground doping concentration and longer carrier lifetime in the absorption region.

IV. CONCLUSION

The comparison of the p-i-n photodiodes for the SWIR/MWIR spectral regions using strain compensated InGaAs/GaAsSb QWs and lattice matched InGaAs/GaAsSb QWs was presented in this paper. The research has shown that the device with 100 pairs of 7 nm In_{0.34}Ga_{0.66}As/5 nm GaAs_{0.25}Sb_{0.75} strain compensated type-II quantum wells as absorption region has an optical response out to 3.4 μm , while the device with 100 pairs of 7 nm In_{0.53}Ga_{0.47}As/5 nm GaAs_{0.5}Sb_{0.5} lattice matched type-II QWs as absorption region has an optical response out to 2.8 μm . The strain compensated devices show detectivity of $2.0 \times 10^8 \text{ cm}\cdot\text{Hz}^{1/2}\cdot\text{W}^{-1}$ at $\lambda = 3.0 \mu\text{m}$ at 290 K and $1.0 \times 10^9 \text{ cm}\cdot\text{Hz}^{1/2}\cdot\text{W}^{-1}$ at 200 K. Also, the carrier transport mechanism in those type-II quantum wells is discussed, but further investigations are needed to clarify all the causes of these phenomena for improving performance on future device development.

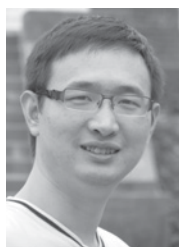
ACKNOWLEDGMENT

The authors would like to thank C. Hu and Z. Lu for their help with measurement of responsivity and noise, and would like to thank A. Liu of IQE for providing the epitaxial wafer.

REFERENCES

- [1] M. Zandian, J. D. Garnett, R. E. Dewames, M. Carmody, J. G. Pasko, M. Farris, C. A. Cabelli, D. E. Cooper, G. Hildebrandt, J. Chow, J. M. Arias, K. Vural, and D. N. B. Hall, "Mid-wavelength infrared p-on-n Hg_{1-x}Cd_xTe heterostructure detectors: 30–120 kelvin state-of-the-art performance," *J. Electron. Mater.*, vol. 32, no. 7, pp. 803–809, 2003.
- [2] J. D. Phillips, K. Moazzami, J. Kim, D. D. Edwall, D. L. Lee, and J. M. Arias, "Uniformity of optical absorption in HgCdTe epilayer measured by infrared spectromicroscopy," *Appl. Phys. Lett.*, vol. 83, no. 18, pp. 3701–3703, Nov. 2003.
- [3] A. Khoshkhalagh, S. Myers, H. Kim, E. Plis, N. Gautam, S. J. Lee, S. K. Noh, L. R. Dawson, and S. Krishna, "Long-wave InAs/GaSb superlattice detectors based on nBn and pin designs," *IEEE J. Quantum Electron.*, vol. 46, no. 6, pp. 959–964, Jun. 2010.
- [4] C. Cervera, J. B. Rodriguez, R. Chaghi, H. Ait-Kaci, and P. Christol, "Characterization of midwave infrared InAs/GaSb superlattice photodiode," *J. Appl. Phys.*, vol. 106, no. 2, pp. 024501-1–024501-5, Jul. 2009.
- [5] S. Mallick, K. Banerjee, S. Ghosh, J. B. Rodriguez, and S. Krishna, "Midwavelength infrared avalanche photodiode using InAs–GaSb strain layer superlattice," *IEEE Photon. Technol. Lett.*, vol. 19, no. 22, pp. 1843–1845, Nov. 2007.
- [6] R.-M. Lin, S.-F. Tang, S.-C. Lee, C.-H. Kuan, G.-S. Chen, T.-P. Sun, and J.-C. Wu, "Room temperature unpassivated InAs p-i-n photodetectors grown by molecular beam epitaxy," *IEEE Trans. Electron Dev.*, vol. 44, no. 2, pp. 209–213, Feb. 1997.
- [7] A. R. J. Marshall, C. H. Tan, M. J. Steer, and J. P. R. David, "Extremely low excess noise in InAs electron avalanche photodiodes," *IEEE Photon. Technol. Lett.*, vol. 21, no. 13, pp. 866–868, Jul. 2009.
- [8] A. Joshi and D. Becker, "High-speed low-noise p-i-n InGaAs photoreceiver at 2- μm wavelength," *IEEE Photon. Technol. Lett.*, vol. 20, no. 8, pp. 551–553, Apr. 2008.
- [9] *Solid State Division* [Online]. Available: <http://www.sales.hamamatsu.com/en/products/solid-state-division/ingaas-pin-photodiodes/long-wavelength-type/part-g8423-03.php>
- [10] R. Sidhu, N. Duan, J. C. Campbell, and A. L. Holmes, Jr., "A long-wavelength photodiode on InP using lattice-matched GaInAs–GaAsSb type-II quantum wells," *IEEE Photon. Technol. Lett.*, vol. 17, no. 12, pp. 2715–2717, Dec. 2005.
- [11] H. Inada, K. Miura, Y. Nagai, M. Tsubokura, A. Moto, Y. Iguchi, and Y. Kawamura, "Low dark current SWIR photodiode with InGaAs/GaAsSb type II quantum wells grown on InP substrate," in *Proc. IEEE Int. Conf. Ind. Phos. Rel. Mater.*, Newport Beach, CA, May 2009, pp. 149–152.

- [12] R. Sidhu, L. Zhang, N. Tan, N. Duan, J. C. Campbell, A. L. Holmes, Jr., C.-F. Hsu, and M. A. Itzler, "2.4 μm cutoff wavelength avalanche photodiode on InP substrate," *Electron. Lett.*, vol. 42, no. 3, pp. 181–182, Feb. 2006.
- [13] D. S. G. Ong, J. S. Ng, Y. L. Goh, C. H. Tan, S. Zhang, and J. P. David, "InAlAs avalanche photodiode with type-II superlattice absorber for detection beyond 2 μm ," *IEEE Trans. Electron Dev.*, vol. 58, no. 2, pp. 486–489, Feb. 2011.
- [14] J. Y. T. Huang, L. J. Mawst, T. F. Kuech, X. Song, S. E. Babcock, C. S. Kim, I. Vurgaftman, J. R. Meyer, and A. L. Holmes, Jr., "Design and characterization of strained InGaAs/GaAsSb type-II 'W' quantum wells on InP substrates for mid-IR emission," *J. Phys. D: Appl. Phys.*, vol. 42, no. 2, pp. 025108-1–025108-8, Jan. 2009.
- [15] W. Y. Jiang, B. Chen, J. Yuan, and A. L. Holmes, Jr., "Design and characterization of strain-compensated InGaAs/GaAsSb type-II MQW structure with operation wavelength at $\sim 3 \mu\text{m}$," *Proc. SPIE: Infr. Technol. Appl. XXXVI*, vol. 7660, p. 76603O, May 2010.
- [16] B. Chen, W. Y. Jiang, J. Yuan, and A. L. Holmes, Jr., "Design of strain compensated InGaAs/GaAsSb type-II quantum well structure for mid-infrared photodiodes," to be published.
- [17] H. D. Vincent, *Fundamentals of Infrared Detector Operation & Testing*, 1st ed. New York: Wiley, Feb. 1990.
- [18] A. Rogalski, "Infrared detectors: Status and trends," *Progr. Quantum Electron.*, vol. 27, nos. 2–3, pp. 59–210, 2003.



Baile Chen received the B.S. degree in physics from the University of Science and Technology of China, Hefei, China, in 2007, and the M.A. degree in physics from the University of Virginia, Charlottesville, in 2009. He is currently pursuing the Ph.D. degree in electrical engineering at the University of Virginia.

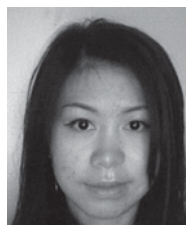
His current research interests include metal-organic chemical vapor deposition growth of III–V semiconductors, designs, fabrication, and characterization of photodetectors and lasers.



Weiyang Jiang received the B.S. degree in physics from Sichuan University, Sichuan, China. He also received the M.S. degree in physics from the University of British Columbia, Vancouver, BC, Canada, and the Ph.D. degree in physics from Simon Fraser University, Burnaby, BC, in 2002 and 2008, respectively.

He has been a Research Associate/Post-Doctoral Fellow in the Department of Electrical and Computer Engineering, University of Virginia, Charlottesville, since 2008. His current research interests include

metal-organic chemical vapor deposition growth of III–V semiconductor photodetectors operating in the mid-infrared regime and also their characterization.



Jinrong Yuan was born in Wuhan, China, on December 24, 1982. She received the B.E. degree in control engineering from the Harbin Institute of Technology, Harbin, China, in 2005. She is currently pursuing the Ph.D. degree in electrical engineering at the University of Virginia, Charlottesville.

Her current research interests include III–V heterojunction p-i-n designs and processing.

Archie L. Holmes, Jr. received the B.S.E.E. degree from the University of Texas, Austin, in 1991, and the M.S. and Ph.D. degrees in electrical engineering from the University of California, Santa Barbara, in 1992 and 1997, respectively.

He joined the Charles L. Brown Department of Electrical and Computer Engineering, University of Virginia, Charlottesville, in 2007. He has co-authored over 95 referred technical articles and has made 66 conference presentations. His current research interests include crystal growth of III-V semiconductors as well as direct wafer bonding for electronic and optoelectronics devices.

Bora M. Onat received the B.S. degree in electronics and telecommunication engineering from Istanbul Technical University, Istanbul, Turkey, in 1992, majoring in microelectronics, and the Ph.D. degree from the Department of Electrical and Computer Engineering, Boston University, Boston, MA, in 1998. His doctoral research involved design, simulation, fabrication, and characterization of high-performance III-V-based photodetectors and arrays for high-speed and polarization sensing applications.

He joined Lucent Technologies Inc., Murray Hill, NJ, in 1998, and became the Lead Designer of seven different production photodiodes for telecom applications and assisted in the development of InP-based avalanche

photodiodes and heterojunction bipolar transistors. In 2001, he joined Celight Inc., Silver Spring, MD, as a Manager, where he was involved in the electro-optic component characterization and developing unique optoelectronic components for coherent telecommunication applications. He started Infinera Inc., Sunnyvale, CA, in 2002, where he led the design and processing of unique InP-based planar light wave circuits and put them into production. He joined Sensors Unlimited, Princeton, NJ, (now a division of Goodrich Corporation) in 2004, where his responsibilities included research and development of epitaxial growth for InP-based devices and program management of multiple government contracts. He is currently a Technical Program Manager at Princeton Lightwave Inc., Cranbury, NJ, leading the effort on epitaxial growth as well as the design and manufacture of photodetectors, photodetector arrays, and lasers in the InP-InGaAs(P) materials system. He has authored over 30 technical papers published in technical journals, conference proceedings, and a book chapter. He holds three U.S. patents.

Dr. Onat is a member of the IEEE Photonics Society (former IEEE Lasers and Electro-Optics Society). He has been a Program Committee Member since 2008. He received the EG&G Photonics Fellowship Award in 1996, the Melles Griot Award in Photonics Research in 1996, and the Department of Education Graduate Assistance in the Area of National Need Fellowship in 1996. Under his leadership, his team was nominated by the Defense Advanced Research Projects Agency (DARPA) for the prestigious Sustained Excellence Award by a Performer Award in 2007 for the successful completion of the DARPA Photon Counting Arrays Program.